TRANSMISSION ELECTRON MICROSCOPE ANALYSIS OF HIGH TEMPERATURE RIMS AROUND TYPE-B CAIs. P. Mane[1], Y. J. Chang[1], P. Wallace[1], and T. J. Zega[1,2], [1]Lunar and Planetary Laboratory, University of Arizona, Tucson, AZ, 85721 (email: pmane@lpl.arizona.edu). [2]Dept. of Materials Science and Engineering, University of Arizona, Tucson, AZ 85721.

Introduction: Relative and absolute dating techniques indicate that calcium-aluminum-rich inclusions (CAIs) are the earliest formed solids in the Solar System [1, 2]. They are composed of high temperature mineral phases that are predicted to have condensed at temperatures starting at ~1750 K [3]. Some CAIs (classified as type-B) show evidence for melting. Most CAIs are surrounded by a sequence of high-temperature multi-mineralic layers [4]. The high-temperaure rims show a general mineralogical sequence of the innermost spinel-perovskite-hibonite layer, followed by melilite-anorthite, Al-rich clinopyroxene and the outermost forsterite layer [4, 5]. Alteration phases such as nepheline, anorthite, sodalite, grossular and wollastonite have also been reported in the rim sequences [6-7]. Incomplete rims around broken CAIs and absence of rims around other chondritic components such as chondrules, suggest restricted spatial or temporal conditions of rim formation in the solar nebula.

The ^{26}Al-^{26}Mg relative dating of the high-temperature rim sequence shows a time of formation varying from 0 to ~2.5 Ma after CAI formation [8-11]. Several mechanisms have been proposed to explain the formation of rims around CAIs, including: 1) condensation and subsequent accretion on the CAI [5, 12-14]; 2) crystallization from a melt, via flash-heating mechanisms [15]; 3) formation as evaporation residues [16]; and 4) growth of layers as a result of chemical gradients set up during alteration of the interior of the inclusion, in nebular settings [7, 17]. Different mineral layers of the rims were likely formed and affected by a combination of these processes. Therefore, a detailed petrographic, chemical, and microstructural analyses of the high-temperature rims can provide better constraints on the environment and conditions in the early Solar System. In order to determine formation mechanism of CAIs and their WL rims, we analyzed a coarse-grained inclusion (CAI-1) from the CV3 chondrite Northwest Africa (NWA) 8323 using transmission electron microscopy (TEM). This study is part of a broader effort to understand the detailed microstructures of CAIs and gain new insight into their origins [5, 18].

Sample Description: NWA 8323 is an oxidized CV3 chondrite that shows a low shock grade and minimal weathering effects [19]. CA-I1 is a coarse-grained type-B inclusion containing melilite, spinel, Ti-rich pyroxene, and anorthite. The WL rim sequence in CAI-1 consists of innermost anorthite, intermediate spinel, and outermost pyroxene layers; in some regions, the rim sequence shows Fe-rich spinel grains and a glassy layer.

The relative ^{26}Al-^{26}Mg ages have been reported for this CAI. The time between formation of CAI-1 interior and its WL rim is $2.2^{+0.7}_{-0.4}$ Ma [11]. Different mineral phases in this CAI range from the CAI end-member ($\Delta^{17}O$ = -25‰) up to the terrestrial value ($\Delta^{17}O$ = 0‰) [11]. The EBSD map of the interior of CAI-1 shows melilite grains with triple junctions suggesting equilibrium conditions during melilite formation [20].

Methods: A petrographic section of the NWA 8323 containing the CAI was examined and three FIB sections of the rim regions sampling three different interfaces were prepared using the FEI Helios Nanolab 660 FIB-SEM located at the University of Arizona. We analyzed these FIB sections using the HF5000, equipped with a cold-field-emission gun, an aberration-corrector for scanning TEM (STEM) imaging, a Gatan Quantum image filter (GIF) ER, and a large solid angle Si-drift Oxford X-max EDS system.

Results and Discussion: FIB Section 1 samples a residual perovskite grain enclosed in melilite and anorthite in the rim layer. The preliminary EDS maps of the section show a thin Fe-rich silicate layer surrounding the perovskite grain. Section 2 samples anorthite-spinel-melilite interface of the high-temperature rim sequence (Figure 1). The EDS data shows that the anorthite is pure $CaAl_2Si_2O_8$ and spinel is $MgAl_2O_4$ with some amount of Fe (up to 2 wt %). The spinel occurs as aggregates of 1 to 2 μm grains. The grain boundaries between anorthite and spinel show a thin layer rich in Fe, Ni and S. The third section samples the grain boundary between spinel-pyroxene layer. While spinels show euhedral 1 to 2 μm grains, the pyroxene layer is fine grained and shows elevated Fe content, suggesting some secondary processes may have affected this layer.

The preliminary EDS data of the FIB of the high-temperature rim sequence sections suggests a complex microstucture of the high-temperature rims. Continued examination of this CAI using TEM techniques will reveal more microstructural details to understand the formation mechanisms of this inclusion and its high-temperature rims.

References: [1] Bouvier A. et al. (2011) GCA, 75(18), 5310-5323. [2] Connelly J. N. et al., (2012) Science, 338(6107), 651-655. [3] Grossman L. (1972) GCA, 36(5), 597-619. [4] Wark D. A. and Lovering J. F. (1977) LPSC VII, 95-112. [5] Bolser D. et al. (2016) MAPS, 51(4), 743- 756. [6] Macpherson G.J. and A.M.

Davis (1993) GCA 57(1), 231-243. [7] MacPherson G. et al. (1982) LPSC XIII. 1079-1091. [8] Simon J.I. et al. (2005) EPSL, 38(3-4), 272- 283.[9] Kawasaki N. et al. (2016) GCA (in press). #2968. [10] Needham A. et al. (2015) 78th Annual Meeting of the Meteoritical Society, Abstract #5014 [11] Mane P. et al. (2016) LPSC XLVII. Abstract #2560. [12] Ito M. and Messenger S. (2008) 71th Annual Meeting of the Meteoritical Society, Abstract #5100. [13] Simon, J.I., et al., (2016) GCA (in press). [14] Simon J.I., et al., (2011) Science, 331(6021), 1175-8. [15] Keller L. et al. (2013) 76th Annual Meeting of the Meteoritical Society, Abstract #5300 [16] Wark D. and Boynton W. V. (2001) MAPS, 36(8), 1135-1166. [17] Ruzicka A. and Boynton, W. (1991) Meteoritics, 26, 39 [18] Zega T. et al. (2016) LPSC XLVII, Abstract #2807. [19] Meteoritical Bulletin, no. 103, in preparation (2014). [20] Mane P. et al. (2017) LPSC XLVIII. Abstract #2968.

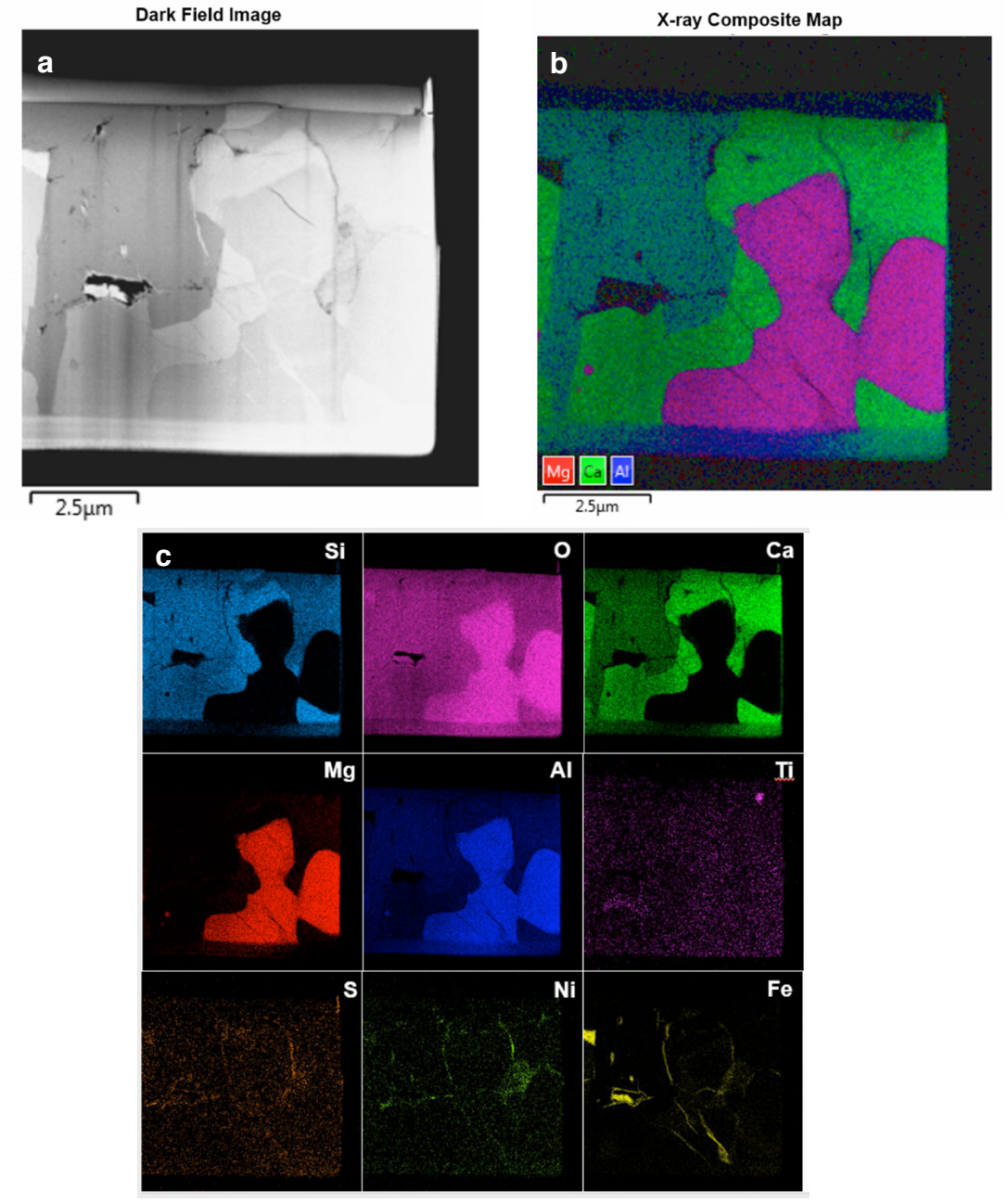

Figure 1: a. Dark field image of section 2. B. EDS composite map showing spinels in pink, melilite in green, and anorthite in blue-green. C. Elemental maps of Section 2.